PHYSICAL REVIEW B **84**, 054509 (2011)

Symmetry-preserving lattice collapse in tetragonal $SrFe_{2-x}Ru_xAs_2$ ($x = 0,0.2$): A combined experimental and theoretical study

Deepa Kasinathan,[1,*] Miriam Schmitt,[1] Klaus Koepernik,[2] Alim Ormeci,[1] Katrin Meier,[1] Ulrich Schwarz,[1]
Michael Hanfland,[3] Christoph Geibel,[1] Yuri Grin,[1] Andreas Leithe-Jasper,[1] and Helge Rosner[1,†]
[1]*Max Planck Institute for Chemical Physics of Solids, Nöthnitzer Str. 40, D-01187 Dresden, Germany*
[2]*IFW Dresden, P.O. Box 270116, D-01171 Dresden, Germany*
[3]*ESRF, BP 220, F-38043 Grenoble Cedex 9, France*

(Received 27 April 2011; published 5 August 2011)

In a joint experimental and theoretical study, we investigate the isostructural collapse from the ambient pressure tetragonal phase to a collapsed tetragonal phase for nonsuperconducting metallic $SrFe_2As_2$ and $SrFe_{1.8}Ru_{0.2}As_2$. The crystallographic details have been studied using x-ray powder diffraction up to 20 GPa pressure in a diamond anvil cell. The structural phase transition occurs at 10 and 9 GPa for $SrFe_2As_2$ and $SrFe_{1.8}Ru_{0.2}As_2$, respectively. The changes in the unit cell dimensions are highly anisotropic with a continuous decrease of the c lattice parameter with pressure, while the a-axis length increases until the transition to a collapsed tetragonal phase and then continues to decrease. Across the phase transition, we observe volume reductions of 5% and 4% for $SrFe_2As_2$ and $SrFe_{1.8}Ru_{0.2}As_2$, respectively. We are able to discern that Ru substitution on the Fe site acts like "chemical pressure" to the system. Density-functional theory-based calculations of the electronic structure and electron localizability indicator are consistent with the experimental observations. Detailed analysis of the electronic structure in k space and real space reveals As $4p_z$ interlayer bond formation as the driving force of the c/a collapse with a change in the As-As bond length of about 0.35 Å.

DOI: 10.1103/PhysRevB.84.054509 PACS number(s): 62.50.−p, 64.60.−i, 71.18.+y, 71.20.−b

I. INTRODUCTION

The surprising discovery of superconductivity in Fe-based pnictides and chalcogenides has steered and revived interest in high-temperature superconductivity.[1] Most of the superconducting members discovered in the past three years can be grouped into five families named by their parent compounds: (i) the 1111 family—ROFeAs/AFeAsF (where R = rare-earth and A = alkaline-earth metal), (ii) the 122 family—AFe_2As_2 (where A = alkaline-earth or divalent rare-earth metal), (iii) the 111 family—AFeAs (where A = alkali metal), (iv) the 11 family—FeSe(Te), and (v) the P22 family—PFe_2As_2 (where P = perovskite oxide such as $Sr_4Sc_2O_6$). The basic common feature of these new parent compounds is the FeAs building block separated by spacer layers comprising the above-mentioned alkali, alkaline-earth, rare-earth oxide or fluoride, or a perovskite oxide.[1–5] Superconductivity is obtained by suitable doping of the parent compounds. For selected recent exhaustive overviews, we refer the readers to Refs. 6 and 7. The thickness of the spacer layers governs the extent of the quasi-two-dimensional (2D) nature of the electronic structure. Using plasma frequencies as a tool to identify the "effective dimensionality" among these systems, it has been shown that the 1111 systems are considerably more 2D than the 122 systems.[8] Interestingly, within these two families a correlation between the dimensionality and the superconducting transition temperature (T_c) can be construed, with the more 2D-like 1111 systems exhibiting a larger T_c than the less anisotropic 122 systems.[8] Superconductivity in these systems upon the suppression of the spin-density-wave (SDW) antiferromagnetic order of Fe can be realized via hole-doping, electron-doping, isovalent substitution, or pressure.[2,9–14] In contrast to doping, high-pressure techniques provide a cleaner route to modify the electronic structure without the added effects of chemical complexity.[15] Many of the high-pressure experiments were focused on investigating the suppression of the Fe-SDW order and the enhancement of T_c. Recently, pressure-induced isostructural transitions from a paramagnetic tetragonal phase (T) to a collapsed tetragonal (cT) phase have been reported for several members of the 122 family: $CaFe_2As_2$, $BaFe_2As_2$, $EuFe_2As_2$, and $EuCo_2As_2$ (Refs. 16–21). The high electronic flexibility of compounds with the $ThCr_2Si_2$-type crystal structure can be related to the subtle interplay of covalent, ionic, and metallic bonding contributions as has been outlined in several previous studies.[22–29] Hoffmann and Zheng[22] also pointed out that in certain cases this might lead to structural phase transitions (see below). Indeed, these structural phase transitions of first and second order have been observed in many AT_2P_2 compounds[30] between two crystallographically isostructural modifications with significantly different P-P distances along the tetragonal c axis. Common to them are the dramatic and highly anisotropic changes in unit cell dimensions (changes of the tetragonal c parameter by −10% and counteracting changes of a by +2%, leading to a collapse of the unit cell volume) depending on temperature,[32] pressure,[30,33–35] composition,[36] and chemical pressure.[37] Curiously, the order of the phase transition (first or second order) was suggested to be dependent on the transition metal atom ($LaFe_2P_2$ being first order and $LaCo_2P_2$ being second order).[30] In contrast, in recent experiments the transition has been reported to be of second order for the arsenides EuT_2As_2 (T = Fe, Co). More systematic studies are necessary to clarify the nature of these transitions, as well as to understand the underlying physics that accompany the formation of the cT phase.

In our joint theoretical and experimental study on $SrFe_2As_2$ and the isovalent Ru substituted sample $SrFe_{1.8}Ru_{0.2}As_2$, we attempt to address a multitude of issues. First, we analyze the possibility of a T → cT phase transition in these systems as has been suggested for many other compounds with ThCr$_2$Si$_2$-type crystal structure. Previous theoretical studies[8,31] have predicted a phase transition from the magnetically ordered orthorhombic SDW phase to a tetragonal phase, but theoretical studies on the T → cT phase transition are rather cursory. Second, we address the nature of the chemical bonding in the 122 arsenides and compare it to the well-studied 122 phosphides. Finally, we challenge the concept of chemical pressure by isovalent substitution of Fe by Ru and study the nature of the isostructural phase transition and the bonding situation of the pnictide. For an isovalent substitution on the Fe site, the As layers remain intact and are unaffected from impurities arising from the substitution elements.

II. METHODS

Polycrystalline samples have been synthesized using solid-state reactions, similar to those described in Refs. 8 and 12. Samples were obtained in the form of sintered pellets. X-ray diffraction measurements (XRD) were performed at the high-pressure beam-line ID09 of the european synchrotron radiation facility up to 20 GPa at room temperature for SrFe$_2$As$_2$ and SrFe$_{1.8}$Ru$_{0.2}$As$_2$. For best possible hydrostatic conditions we used a membrane diamond anvil cell (DAC) with helium as the pressure-transmitting medium. The pressure was determined using the ruby fluorescence method. The measured powder rings were integrated using the program FIT2D.[38] After a background correction the lattice parameters were determined with the FullProf[39] package.

Density-functional theory-based band-structure calculations were performed using a full-potential all-electron local-orbital code FPLO[40,41] within both the local density approximation (LDA) as well as the generalized gradient approximation (GGA). Relativistic effects were incorporated on a scalar-relativistic level. A well-converged k mesh with 24^3 points in the full Brillouin zone was used. The crystal structures were optimized at different levels to investigate or isolate effects that may depend sensitively to certain structural features. The full relaxation of the unit cell involves optimizing the c/a ratios in addition to relaxing the z(As) coordinate. The electron localizability indicator/function (ELI/ELF) was evaluated according to Ref. 42 with an ELI/ELF module implemented within the FPLO program package.[43] The topology of ELI was analyzed using the program BASIN[44] with consecutive integration of the electron density in basins, which are bound by zero-flux surfaces in the ELI gradient field. This procedure, similar to the one proposed by Bader for the electron density,[45] allows us to assign an electron count for each basin.

III. RESULTS AND DISCUSSION

A. Symmetry-preserving lattice collapse

1. Experiment: SrFe$_2$As$_2$

Collected in Fig. 1 are the measured tetragonal lattice parameters a and c, the axial ratio c/a, and the unit cell volume as a function of increasing pressure for the parent compound SrFe$_2$As$_2$ (with the 10% Ru-doped SrFe$_{1.8}$Ru$_{0.2}$As$_2$ being addressed later in this report).[46] For SrFe$_2$As$_2$, the lattice parameters a and c show an initial decrease with pressure up to 5 GPa. Upon further increase in pressure, anomalous compression effects are observed with the lattice parameter a expanding rapidly up to around 10 GPa, while the c lattice parameter continues to decrease. At this juncture a strong decrease is witnessed in the c lattice parameter to smaller values (a transition from a T to a cT phase), after which a normal compression behavior is observed up to 20 GPa. The c/a ratio as a function of pressure shows the onset of the structural phase transition around 10 ± 1 GPa from a T phase (with $c/a \approx 2.85$) to a cT phase (with $c/a \approx 2.65$). Refer to Tables I and II in the supplementary information for more details.

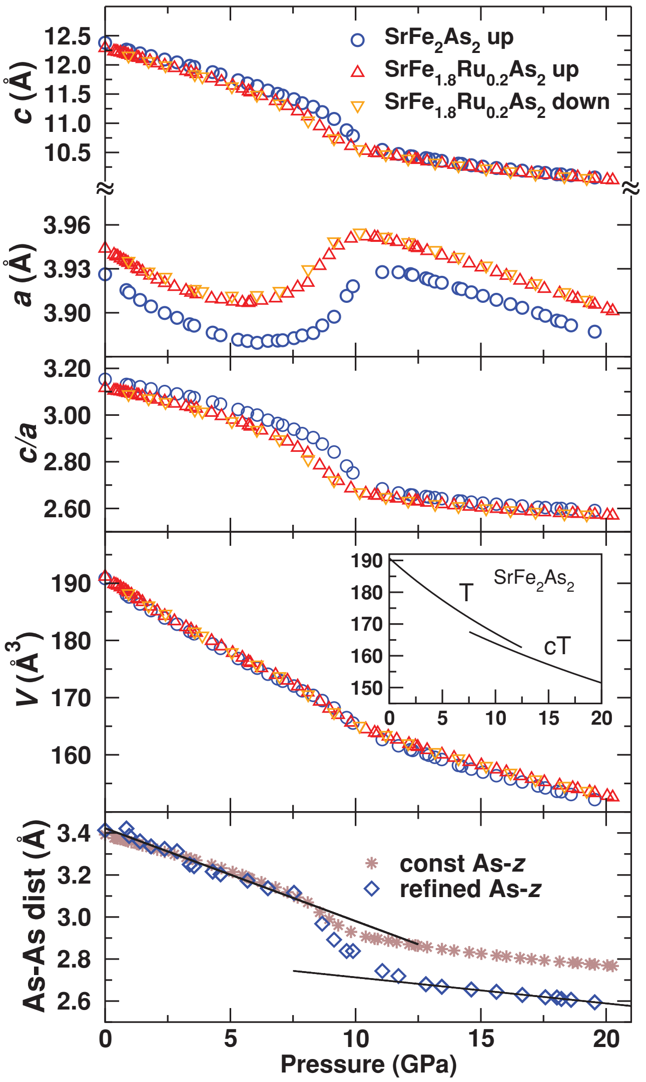

FIG. 1. (Color online) The measured tetragonal lattice parameters a and c, the axial ratio c/a, and the unit cell volume as a function of applied pressure for SrFe$_2$As$_2$ and SrFe$_{1.8}$Ru$_{0.2}$As$_2$. The measurements were performed at room temperature. The inset shows the Birch-Murnaghan equation of state fitting for the tetragonal (T) and collapsed (cT) phase for SrFe$_2$As$_2$. The lowest panel displays the As-As distance for SrFe$_2$As$_2$ obtained from a full refinement of the z coordinate of the As atoms. To separate the influence due to the decrease in c, only, the As-As distance using the z coordinate of As at ambient pressure is also shown.

Similarly, an abrupt change in the interlayer As-As distance was observed. However, this change of the interlayer distance can be accounted for only partially by the change of the lattice parameter c (see Fig. 1, lower panel). This distance decreases from the rather large value of 3.41 Å (at ambient pressure) to a value of 2.59 Å (at the highest measured pressure of 19.6 GPa). Similar interatomic distances are found for example in skutterudite $CoAs_3$ (2.49/2.56 Å)[47] or filled skutterudite $LaFe_4As_{12}$ (2.57/2.58 Å).[48] These values are only slightly larger than the single-bond distance of 2.52 Å occurring in α-As.[49] The collapse of the lattice is, in turn, also accompanied by a simultaneous pronounced decrease of the Sr-As distances d_{SrAs} and Fe-As distances d_{FeAs} by about 12% and 4%, respectively, as well as decreases in the angles in the $FeAs_4$ tetrahedron. Electronic structure calculations have shown that even minute shifts in z(As) and thus the resulting Fe-As distances have strong impact on the occupation of the Fe $3d_{x^2-y^2}$ orbitals and therefore the magnetic behavior in the $A\mathrm{Fe}_2\mathrm{As}_2$ phases.[21,50] These effects should become even more magnified during the observed phase transition. In contrast, under applied external pressures up to 6 GPa, a pronounced robustness of the Fe-As bonds is recognized for $BaFe_2As_2$,[51] which crystallizes with a significantly larger c/a ratio of 3.35. However, the Ba-As distances significantly contract (by about 3%).

The measured pressure-volume data were fit using a Birch-Murnaghan equation of state for the two separate phases (shown as an inset in Fig. 1). The obtained equilibrium volume V_0, bulk modulus B_0, and its pressure derivative B' for the tetragonal phase (0–8.6 GPa) are $V_0 = 190.7$ Å^3, $B_0 = 63.63$ GPa, and $B' = 2.51$, respectively, and for the collapsed tetragonal phase (11–19.5 GPa) they are $V_0 = 180.8$ Å^3, $B_0 = 89.57$ GPa, and $B' = 2.51$, respectively. Our observation of the T → cT phase transition in $SrFe_2As_2$ along with the anisotropic compressibility phenomena is akin to the reports on other 122 arsenides AT_2As_2 (A = Ca, Ba, Eu; T = Fe, Co).[16–21]

2. Calculations: $SrFe_2As_2$

Previous work on the tetragonal collapse in other members of the $A\mathrm{Fe}_2\mathrm{As}_2$ family (A = Ca, Ba, and Eu) have mostly been experimental studies.[17–20] Analysis of the electronic structure of the Fe-As-based systems using band-structure calculations has been quite successful in describing certain "general trends" such as the tetragonal to orthorhombic structural distortion, reduction in the magnetic moment as a function of doping, etc., though density functional theory (DFT) is less accurate in reproducing certain details such as the Fe-As bond length.[8] In 2009, Yildirim reported on results from first-principles calculations for $CaFe_2As_2$ and noted that the formation of the cT phase is controlled by the Fe-spin state.[52] He suggested that pressure reduces the Fe-spin moment, which in turn weakens Fe-As bonding and strengthens the As-As interaction and therefore causes the collapse of the lattice parameters. Here, also using first-principles calculations, we decouple Fe magnetism from the chemical bonding scenario and elucidate the bond formation as the key feature. To realize this, we calculated the change in the ground-state energy as a function of volume employing both the LDA and the GGA and using the tetragonal symmetry without invoking spin degrees of freedom explicitly. At each volume two kinds of optimization were performed, one in which only the c/a ratio was optimized and another in which a simultaneous optimization of the z(As) position was additionally carried out. Collected in Fig. 2 are the a and c lattice parameters and the c/a ratio as a function of volume obtained using the LDA with only c/a optimization.[53] The calculations reproduce the experimental results including the transition from the ambient-pressure T phase to the cT phase for $SrFe_2As_2$ in accord with a dramatic jump in the axial ratio c/a from 2.85 to 2.65. Our calculations also reproduce the observed anomalous expansion of the lattice parameter a under pressure. This is the first theoretical observation of the anomalous expansion phenomena in the nonmagnetic tetragonal symmetry for the FeAs family of materials.[54] By fitting the energy-volume (E-V) curves to two separate Birch-Murnaghan equations of state (EOS) fits (not shown here), we obtain a transition pressure of 11 ± 1 GPa. The pressure (P) is obtained from the volume derivative of the EOS, which is inverted to get $V(P)$. Equating the enthalpies $E[V(P)] + PV(P)$ of the two phases gives the transition pressure. The calculated value is in good agreement with the experimental value of 10 ± 1 GPa. Calculations using GGA (see Fig. 1. in supplementary information)[53] with only c/a optimization give essentially the same trend for a, c, and c/a as described above for the LDA.

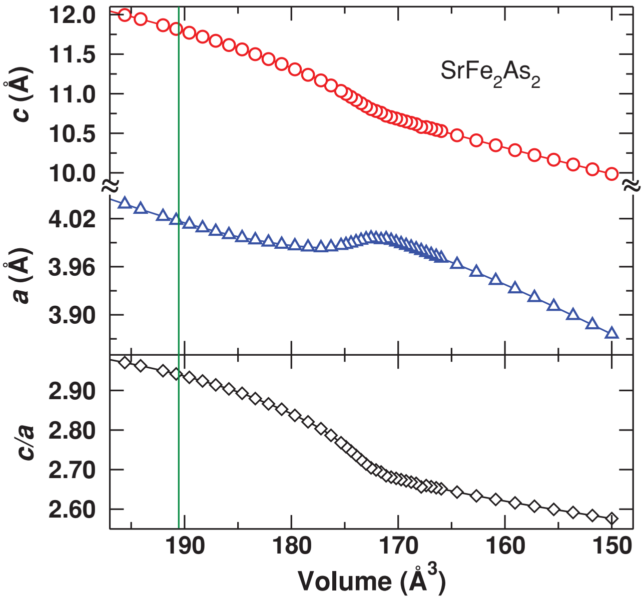

FIG. 2. (Color online) Calculated a, c, and c/a as a function of unit cell volume for $SrFe_2As_2$ within the LDA. At each volume, only the c/a optimization has been performed. The c lattice parameter decreases throughout, while the a lattice parameter undergoes an anomalous expansion for some reduced volumes before it continues to decrease again. The vertical line denotes the experimental ambient condition volume.

Relaxing additionally the z(As) position worsens the quantitative description for both the LDA and the GGA. This behavior is not surprising because, as mentioned previously, the Fe-As bond length is quite sensitive and DFT fails in accurately reproducing the experimental Fe-As bond length even for ambient conditions.[55,56] Another inadequacy of DFT that is worth mentioning here is the equilibrium volume. It is well known that the LDA and the GGA usually underestimate and overestimate, respectively, the equilibrium volume by just a few percent as compared to experiments. For $SrFe_2As_2$ the LDA and the GGA underestimate the equilibrium volume by 17% and 10%, respectively. This is quite unusual and at present there exists no conclusive reasoning for such a behavior. One possible explanation that is gaining more acceptance is the presence of a nematic order, which is unaccessible using the present-day DFT tools.[57]

3. *Experiment: $SrFe_{1.8}Ru_{0.2}As_2$*

Similar to hydrostatic external pressure, studies on the effects of substitution on the transition metal Fe site also show anisotropic changes in the lattice parameters, with a significant contraction of the c-axis length as compared to a.[10–12,58] For example, substitution of Fe with the isovalent, but larger Ru atom does not introduce any additional charge into the system and is suggested to simulate the effect of “chemical pressure,” alluding to the possibility of observing a T → cT phase transition in this substitution series. For the substitution series $SrFe_{2-x}Ru_xAs_2$ $(0 \leqslant x \leqslant 2)$, a significant but monotonic contraction of the lattice parameter c was reported, though no clear phase transition from a T phase to a cT phase was observed.[12] The lack of a phase transition in $SrFe_{2-x}Ru_xAs_2$ could be a consequence of substitutional disorder in the samples and the model of a chemically induced pressure volume effect is most likely an oversimplified assumption.[59] Nevertheless, we wanted to discern the idea of Ru substitution acting as a chemical pressure. To this end, we have collected the pressure dependence of the structural parameters a, c, and c/a and unit cell volume for a 10% Ru-doped sample $SrFe_{1.8}Ru_{0.2}As_2$ (see Fig. 1). We have chosen a rather small Ru content to keep the impurity and disorder effects to a minimum. At room temperature and pressure, $SrFe_{1.8}Ru_{0.2}As_2$ is in the T phase with $c/a \approx 3.1$. Similar to the parent compound, this sample is also metallic and nonsuperconducting at ambient pressure. Upon application of pressure, the system also shows a transition to a cT phase, though the transition pressure is shifted downward ($\approx 9 \pm 1$ GPa) as compared to $SrFe_2As_2$ (see Tables III and IV in supplementary information for more details).[53] The observed hysteresis loop between pressure-up and pressure-down data (see Fig. 1, top panel, upward and downward triangles for pressure up and down, respectively) is rather small, similar to the measurements on $CaFe_2As_2$ and $BaFe_2As_2$.[17] A fit to a Birch-Murnaghan equation of state was done for the tetragonal and the collapsed tetragonal phases. The obtained equilibrium volume, bulk modulus B_0, and its pressure derivative B' for the tetragonal phase (0–7.3 GPa) are $V_0 = 191.2$ Å^3, $B_0 = 63.3$ GPa, and $B' = 2.85$, respectively, and for the collapsed tetragonal phase (9–20 GPa) they are $V_0 = 183.1$ Å^3, $B_0 = 83.6$ GPa, and $B' = 2.86$, respectively. Comparing the experimental results of $SrFe_2As_2$ and $SrFe_{1.8}Ru_{0.2}As_2$, we can now perceive that the 10% Ru substitution did indeed act as a chemical pressure in the sample and reduced the external pressure needed for inducing a T → cT phase transition in $SrFe_{1.8}Ru_{0.2}As_2$ to 9 GPa as compared to the 10 GPa pressure needed for the (Ru-free) $SrFe_2As_2$ sample.[60]

4. *Calculations: $SrRu_2As_2$*

The bonding scenario for Ru in the end member of the substitution series $SrRu_2As_2$ is similar to that of Fe in $SrFe_2As_2$. Moreover, $SrRu_2As_2$ is nonmagnetic at ambient conditions in contrast to the paramagnetic $SrFe_2As_2$. Analyzing the effects of external pressure in $SrRu_2As_2$ will therefore isolate all other parameters and provide a purely chemical picture of the transition. The c/a ratio of $SrFe_2As_2$ is $\approx$3.15 at ambient conditions and $\approx$2.65 for the cT phase. In contrast, $SrRu_2As_2$ has a ratio $c/a \approx 2.68$ at room temperature[61] and ambient pressure, and therefore it is already in the cT phase at ambient conditions. Therefore, the effect of external pressure on $SrRu_2As_2$ must be much weaker compared to $SrFe_2As_2$. Collected in Fig. 3 are the changes in the lattice parameters a, c, and c/a obtained from LDA calculations as a function of volume. Both a and c decrease rather monotonically with the decrease in volume and do not show any intermediate anomalous expansion of the a lattice parameter. Moreover, in contrast to the calculated results obtained above for $SrFe_2As_2$ and in accordance to the generally accepted trend, the LDA slightly underestimates and the GGA (Fig. 2. in supplementary information)[53] slightly overestimates the equilibrium volume with respect to the experiment.[12,61]

Since this phase transition is not connected with a change in the symmetry, the nature of the transition can be first or second order, or even a continuous crossover. Moreover, the transition might be first order at $T = 0$, but if the critical end point terminating the cT(P) phase boundary line is below 300 K, one would only observe a continuous crossover at 300 K. The signatures expected for a first-order transition, a second-order one, and a crossover are, respectively, a jump, a jump in the

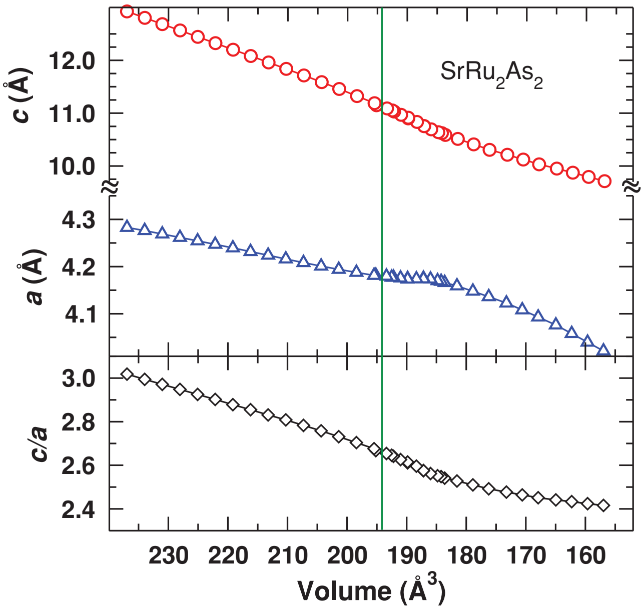

FIG. 3. (Color online) Calculated a, c, and c/a as a function of unit cell volume for $SrRu_2As_2$ within the LDA. At each volume, only the c/a optimization has been performed. The vertical line denotes the experimental ambient condition volume.

derivative, and an S-shaped behavior in the relevant property, in the present case, the c/a ratio. The data presented in Fig. 1 do not evidence a sharp jump; instead, they clearly suggest a jump in the derivative $d(c/a)/dT$, especially for pure $SrFe_2As_2$. Thus the present data indicate the transition in $SrFe_2As_2$ to be of second order, instead of the well-established first-order type in $CaFe_2As_2$.[16] This difference between $CaFe_2As_2$ and $SrFe_2As_2$ is in line with LDA calculations for the difference in the evolution of the total energy as a function of decreasing volume and c/a, where a second local minimum in $E(c/a)$ is much more pronounced in $CaFe_2As_2$ than in $SrFe_2As_2$.[8]

B. Chemical bonding

Ternary compounds AT_2X_2 crystallizing with the tetragonal $ThCr_2Si_2$ type of structure[62] are numerous[63,64] and have been the focus of experimental and theoretical studies in solid-state sciences for several decades.[65] This research originated with investigations on the Si- and Ge-based family of AT_2X_2 compounds,[62,66,67] and later embraced pnictogens as X elements.[68–72] That pnictogen-based members of this family of compounds are always good for a surprise has already been recognized with the discovery of superconducting $LaRu_2P_2$ ($T_c = 4.1$ K) more than two decades ago.[73] The crystal structure comprises T_2X_2 layers with edge-sharing TX_4 tetrahedra parallel to the ab plane. These layers are additionally separated by planes of metal atom A (as can be seen in Fig. 7). Systematic structural and chemical observations early on have resulted in classifying the AT_2X_2 compounds adopting the $ThCr_2Si_2$ structure type into two branches: (i) One, with a three-dimensional network built up of tetrahedral TX_4 layers, is held together by X-X bonds along the c axis (with two apex X atoms from two adjacent layers forming the bond), with the A atoms embedded between these layers. This structural peculiarity has been mainly observed for silicides and germanides.[64] This branch is usually described as the $ThCr_2Si_2$ or $CeGa_2Al_2$ type. (ii) The other branch exhibits a rather two-dimensional layered structure with large separations between the X atoms along the c axis. This branch is described as the $TlCu_2Se_2$ type. Interestingly, depending on the transition metal T, compounds containing pnictogens (well documented for phosphides) have been found to belong to both branches and to intermediate cases. Variation and substitution of the transition metal T (increasing the number of d electrons) or the metal atom A have been discovered as a means of tuning this structural peculiarity by causing a shrinkage of the X-X distances and bringing the X species in close bonding contacts. Furthermore, it had also been discerned that the geometrical constraints due to the changes in the sizes of the constituent atoms alone was not adequate to facilitate the X-X bond formation. These analyses early on evoked questions about the electronic structure governing the underlying bonding situations[71,74] and the observed physical properties.[72,75,76] The absence of pnictogen-pnictogen bonds indicated by large c/a ratios leads to a composite-like structural arrangement of the $[T_2X_2]$ layers held together by more or less ionic interactions mediated by the electropositive A cations. Members of the $TlCu_2Se_2$ branch could therefore be qualitatively described within the Zintl concept[77] by assigning a formal oxidation number -3 to the most electronegative element (pnictogen) resulting in a polyanion $[T_2X_2]^{2-}$ counterbalanced by a cation A^{2+} (e.g., $Sr^{2+}Fe^{2+}Fe^{2+}P^{3-}P^{3-}$). In contrast, compounds of the $ThCr_2Si_2$ family exhibiting pnictogen-pnictogen bonds are preferentially formed by the late transition metals. The corresponding qualitative view in light of the Zintl concept is now based on diatomic $[X_2]^{4-}$ entities (e.g., $Ca^{2+}Ni^{1+}Ni^{1+}[P_2]^{4-}$ as discussed in Refs. 73 and 75). However, regarding the T-T bonding interactions a slightly different trend was inferred from atomic distances and occupation of simple and idealized molecular orbital schemes, suggesting a more pronounced covalency for Fe-Fe bonds than for Ni-Ni bonds (Refs. 78–80). In a similar way of reasoning the chemical bonding was qualitatively rationalized in As-based compounds.[72,75] Hoffmann highlighted this genuine occurrence of making and breaking of a diatomic (X-X) bond in the solid state for the AT_2X_2 structures and pioneered the investigation of the chemical bonding situation in phosphides based on extended Hückel calculations, discovering structural flexibility due to a subtle interplay between pnictogen-pnictogen and pnictogen-metal bonding with the additional ingredient of packing requirements of the large A atoms.[22]

1. Chemical bonding in k space

In order to investigate the development of an interlayer chemical bond between As p_z orbitals in $SrFe_2As_2$ as we go from the ambient-pressure T phase to the cT phase, we analyze the orbital character of the band structure ("fat bands"). Usually, fat bands are obtained by suitable projection of the extended wave function onto test orbitals with a certain character, which in a local-orbital code naturally are chosen to be the local orbitals themselves. Atom-centered projectors do not probe the phase relations between different sites, though. In order to obtain this phase information, which contains the chemical interpretation in terms of bonding characteristics, projectors containing several sites are needed. We choose projectors which include As $4p_z$ orbitals of a pair of As atoms sitting on top of each other across the Sr interlayer spacer. The two combinations are bonding $\Phi_\sigma = \frac{1}{\sqrt{2}}(\Phi_1 - \Phi_2)$ and antibonding $\Phi_{\sigma^*} = \frac{1}{\sqrt{2}}(\Phi_1 + \Phi_2)$ within the pair. Here, the negative sign gives bonding because of the odd parity of the p orbitals. The corresponding fat bands probe the phase correlation between the two As p_z orbitals but do not probe the phase between pairs of As atoms within the layer. Due to the unitarity of the transformation from orbitals to projectors the resulting bonding and antibonding orbital weights sum to the "standard" orbital-projected weights, which opens up the possibility of analyzing not only the band structure but also the projected density of states according to bonding characteristics.

Figure 4 shows the σ and σ^* fat bands for the ambient-pressure T phase and for the high-pressure cT phase of $SrFe_2As_2$. In both phases the bonding part of the $4p_z$ bands (green or light gray) are mostly occupied. In the T phase the antibonding bands are significantly occupied, while they get pushed up close to and above the Fermi level in the cT phase. There is one antibonding band remaining below the Fermi level; however, the total weight of occupied antibonding bands is strongly reduced for the cT phase as compared to the T phase.

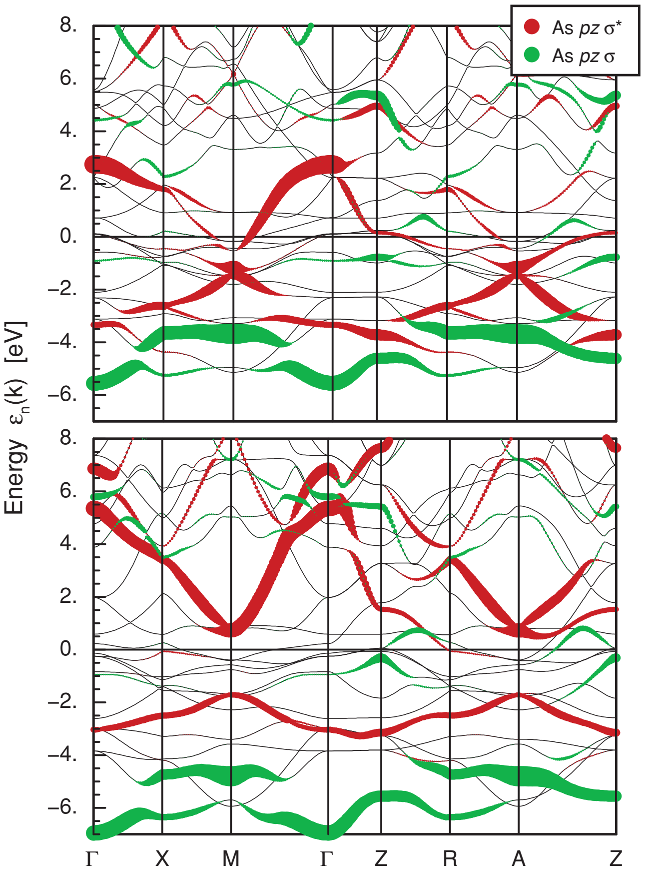

FIG. 4. (Color online) Bonding (σ, green or light gray) and antibonding (σ^*, red or dark gray) As $4p_z$ "fat bands" for $SrFe_2As_2$. The Fermi level is at 0 eV. Upper panel: T phase. Lower panel: cT phase.

In order to quantify the bond strength we plot the difference of the integrated σ and σ^* projected density of states (DOS) along with the projected DOS in Fig. 5. In an idealized case of completely occupied bonding and completely unoccupied antibonding states this difference of energy-resolved occupations will be monotonically increasing up to a value of two (spin degeneracy) at the chemical potential, signifying that two electrons form the bond, and will monotonically decrease with increasing energy away from the Fermi level, to reach zero if all bands are filled with a total number of four electrons. The value of this difference occupation at the Fermi level is an estimate of chemical binding in terms of excess bonding electrons (EBE). Figure 5 shows that the number of EBE is only 0.4 in the T phase but is reaching nearly 1 in the collapsed phase. It turns out that the number of EBE increases by ≈0.7 immediately before the collapse occurs, showing that the driving force of the collapse is the onset of $4p_z$ interlayer bond formation.

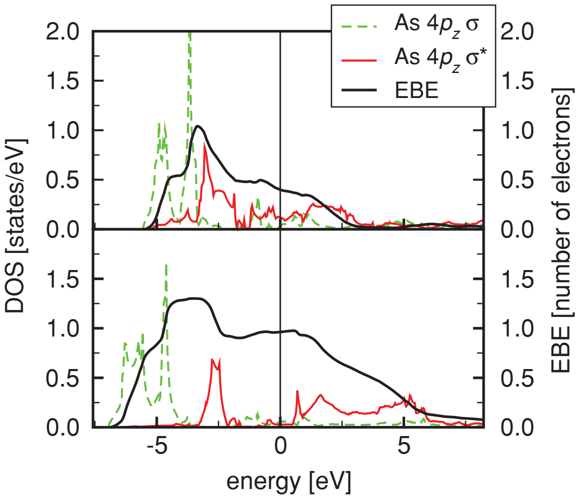

FIG. 5. (Color online) The σ (dashed, green color or light gray) and σ^* (solid, red color or dark gray) density of states for the T phase (upper panel) and for the cT phase (lower panel) of $SrFe_2As_2$. The solid (black) line shows the number of excess bonding electrons, EBE (see text for explanation).

Besides the increased band width in the cT phase compared to T phase, there are additional changes occurring at the Fermi level. In the T phase there is a strongly antibonding band starting at -0.5 eV at the M point going to 3 eV at the Γ point. This band is hybridized with the Fe $3d_{x^2-y^2}$ orbitals. In the cT phase this particular band now begins at around 1 eV above the Fermi level and has a larger dispersion going up to 7 eV. Most importantly, this band, which formed a Fermi surface in the T phase, gets removed from the Fermi level for the cT phase, which results in a change of the Fermi surface topology (Fig. 6). In general the Fe bands do not change as drastically as the As bands across the transition. Most notably the Fe band width is not following the strong increase of the As band width. From a chemical point of view, the Fe layer stays inactive in the collapse. However, from a physical point of view, the Fe bands, especially the Fermi surface, changes from a 2D to a 3D system. Of the two cylindrical

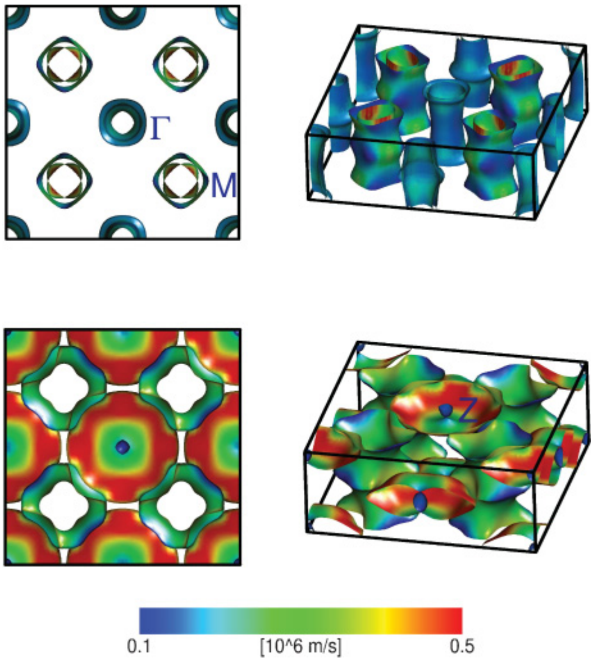

FIG. 6. (Color online) Fermi surfaces for the tetragonal T (upper panel) and collapsed tetragonal cT (lower panel) phases. The color code shows the magnitude of the Fermi velocity.

sheets around the M point (T phase) only one remains after the collapse, while of the three cylinders around Γ one vanishes, the second becomes a very small pocket, and the third forms a large pocket around the Z point. This large pocket shows a quite three-dimensional distribution of Fermi velocities. The plasma frequencies change from $\Omega_{xy} = 2.81$ eV and $\Omega_z = 0.96$ eV in the T phase to $\Omega_{xy} = 2.56$ eV and $\Omega_z = 3.81$ eV in the cT phase. In fact the ratio λ between in-plane and out-of-plane plasma frequencies goes from $\lambda \approx 3$ to $\lambda \approx 0.7$. Interestingly, the individual bands behave rather differently. The still more cylindrical band around M has a ratio $\lambda \approx 1.2$ while the pocket around Z has $\lambda \approx 0.48$, which makes this band actually tend to be more one dimensional along the z axis, which is another aspect in the formation of interlayer As-As bonds.

2. Chemical bonding in real space

The electron localizability indicator (ELI, Υ) was evaluated in the ELI-D representation according to Refs. 42 and 81 with an ELI-D module. The ELI-D distribution for the ambient condition T phase shown in the upper panel of Fig. 7 has four distinct features. The valence (fifth) shell[82] of the Sr atoms is absent, suggesting the formation of the Sr cation and the transfer of these electrons to the $[Fe_2As_2]$ anion. The penultimate (fourth) shell of Sr is not specially structured,[83,84] indicating that the electrons of this shell do not participate in the bonding interactions in the valence region. Between the As atoms, two distinct maxima of ELI-D are observed, illustrating the absence of As-As bonds and the nonbonding (lone-pair-like) interaction between the neighboring $[Fe_2As_2]$ anions. The structuring of the penultimate (third) shell of the Fe atoms toward the closest As is the fingerprint of the Fe-As bonding within this anion. For the high-pressure cT phase (lower panel of Fig. 7), in addition to the Coulomb interaction between the Sr cations and the $[Fe_2As_2]$ anions, there is also bonding by the electrons of the penultimate (fourth) Sr shell (cf. structuring of this shell in Fig. 7, lower panel). This observation is similar to the one for Eu in $EuRh_2Ga_8$.[85] The distinct maxima found close to the Fe-As contacts (ELI-D isosurface with $\Upsilon = 1.24$) shows the formation of covalent bonds within the $[Fe_2As_2]$ anion. The formation of the As-As bonds between the neighboring anions is visualized in real space by a concentration of ELI-D close to the middle point of the As-As contact (ELI-D isosurface with $\Upsilon = 1.18$), which is very similar in topology to the ELI-D distribution in the simple example of the F_2 molecule.[86,87]

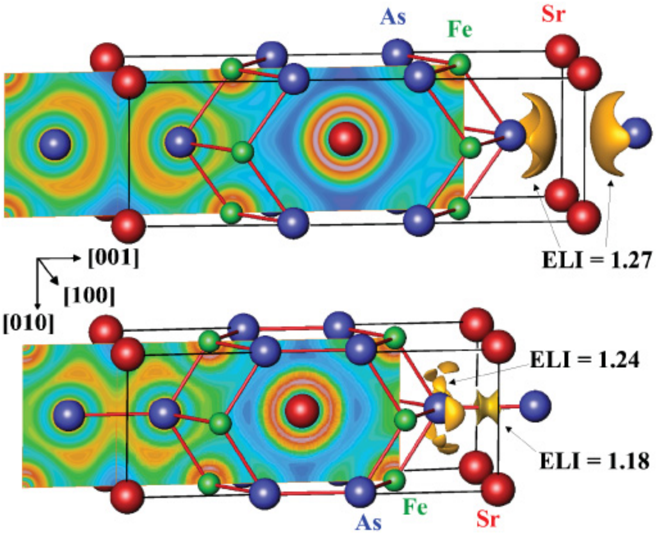

FIG. 7. (Color online) ELI-D of the ambient-pressure T phase (top panel) and the cT phase at high pressure (bottom panel) of $SrFe_2As_2$. The slices in the left part reveal the distribution of ELI-D between the As atoms. The absence of As-As bonding in the T phase is illustrated by the isosurfaces of $\Upsilon = 1.27$, while the formation of As-As bonds in the cT phase is illustrated by the isosurfaces of $\Upsilon = 1.18$.

IV. SUMMARY

In conclusion, we have studied the transition under high pressure from a tetragonal to a collapsed tetragonal phase in $SrFe_2As_2$ and $SrFe_{1.8}Ru_{0.2}As_2$, using diamond anvil cells and powder XRD measurements up to 20 GPa at room temperature. We observe an isostructural phase transition from a T phase to a cT phase at 10 GPa for $SrFe_2As_2$ and at 9 GPa for $SrFe_{1.8}Ru_{0.2}As_2$. Both materials show an anomalous compression behavior (anisotropic changes in the unit cell dimensions) under pressure with the lattice parameter c decreasing continuously while the lattice parameter a increases for a certain pressure range. Our observation is akin to previous reports[16–20] on other 122 systems AT_2As_2 (A = Ca, Ba, Eu; T = Fe, Co). From our experiments, we note that Ru substitution of the Fe site works as "chemical pressure," thereby reducing the amount of external pressure needed to obtain the T → cT phase transition in $SrFe_{1.8}Ru_{0.2}As_2$. Band structure calculations reproduce the isostructural phase transition observed in experiments, including the anisotropic changes in the unit cell dimensions. Detailed analyses in k space (of Fermi surfaces, band structure, and density of states) as well as in real space (ELI-D) of the bonding scenario within and between the FeAs layers in both the T and cT phases presently provide a comprehendible picture of the driving force behind the observed lattice collapse. The actual phase transition can be rationalized in the following way. Since the covalently bonded rather rigid transition metal-pnictogen layers are separated by the large cations (e.g., Sr^{2+}), short As-As bonds along the c axis cannot be formed due to geometric reasons in the ambient-pressure T phase. The predominantly ionic interaction between the cations and the polyanion makes these layered compounds soft along the stacking c axis. Thus, applying pressure leads to a decrease of the distance between the layers and therefore the As-As separation. When a critical As-As distance is reached to enable a sufficiently high enough orbital overlap of the $4p_z$ orbitals, promptly the bonding interactions dominate and the phase transition occurs. Similar to the case previously studied for phosphorus-based compounds,[25,32] electronic structure calculations outline a scenario where a stabilization of the As-As bonding states stabilizes Fe-As antibonding states which have lifted up the former ones to energies near the Fermi level. Consequently, the Fe-As bonds become weaker and the lattice parameter a increases whereas c decreases at the phase transition.

Note added in proof. While revising the manuscript, we became aware of another recent experimental work on the tetragonal collapse in $SrFe_2As_2$ under nonhydrostatic conditions.[88] Consistent with our experimental data under hydrostatic conditions, the authors observed a transition to the collapsed tetragonal phase at room temperature at 10 GPa.

ACKNOWLEDGMENTS

We acknowledge stimulating discussions with W. Schnelle. This research has been partly funded by DFG within SPP 1458. We thank H. Borrmann and U. Burkhardt for performing powder x-ray diffraction and metallographic characterization as well as electron probe micro analysis of the samples used in this study.

---

[*] deepa.kasinathan@cpfs.mpg.de

[†] helge.rosner@cpfs.mpg.de

[1] Y. Kamihara, T. Watanabe, M. Hirano, and H. Hosono, J. Am. Chem. Soc. **130**, 3296 (2008).

[2] M. Rotter, M. Tegel, and D. Johrendt, Phys. Rev. Lett. **101**, 107006 (2008).

[3] H. S. Jeevan, Z. Hossain, D. Kasinathan, H. Rosner, C. Geibel, and P. Gegenwart, Phys. Rev. B **78**, 092406 (2008).

[4] F. C. Hsu *et al.*, Proc. Natl. Acad. Sci. USA **105**, 14262 (2008).

[5] H. Ogino, Y. Matsumura, Y. Katsura, K. Ushiyama, S. Horii, K. Kishio, and J. Shimoyama, Supercond. Sci. Technol. **22**, 075008 (2009).

[6] D. C. Johnston, Adv. Phys. **59**, 803 (2010).

[7] Y. Mizuguchi and Y. Takano, J. Phys. Soc. Jpn. **79**, 102001 (2010).

[8] D. Kasinathan, A. Ormeci, K. Koch, U. Burkhardt, W. Schnelle, A. Leithe-Jasper, and H. Rosner, New J. Phys. **11**, 025023 (2009).

[9] H. S. Jeevan, Z. Hossain, D. Kasinathan, H. Rosner, C. Geibel, and P. Gegenwart, Phys. Rev. B **78**, 052502 (2008).

[10] A. S. Sefat, R. Jin, M. A. McGuire, B. C. Sales, D. J. Singh, and D. Mandrus, Phys. Rev. Lett. **101**, 117004 (2008).

[11] A. Leithe-Jasper, W. Schnelle, C. Geibel, and H. Rosner, Phys. Rev. Lett. **101**, 207004, (2008).

[12] W. Schnelle, A. Leithe-Jasper, R. Gumeniuk, U. Burkhardt, D. Kasinathan, and H. Rosner, Phys. Rev. B **79**, 214516 (2009).

[13] S. Sharma, A. Bharati, S. Chandra, V. R. Reddy, S. Paulraj, A. T. Satya, V. S. Sastry, A. Gupta, and C. S. Sundar, Phys. Rev. B **81**, 174512 (2010).

[14] C. F. Miclea, M. Nicklas, H. S. Jeevan, D. Kasinathan, Z. Hossain, H. Rosner, P. Gegenwart, C. Geibel, and F. Steglich, Phys. Rev. B **79**, 212509 (2009).

[15] C. W. Chu and B. Lorenz, Physica C **469**, 385 (2009).

[16] A. Kreyssig *et al.*, Phys. Rev. B **78**, 184517 (2008).

[17] R. Mittal *et al.*, e-print arXiv:1007.2320.

[18] W. Uhoya *et al.*, Phys. Rev. B **82**, 144118 (2010).

[19] W. Uhoya, G. Tsoi, Y. K. Vohra, M. A. McGuire, A. S. Sefat, B. C. Sales, D. Mandrus, and S. T. Weir, J. Phys. Condens. Matter **22**, 292202 (2010).

[20] M. Bishop, W. Uhoya, G. Tsoi, Y. K. Vohra, A. S. Sefat, and B. C. Sales, J. Phys. Condens. Matter **22**, 425701 (2010).

[21] A. I. Goldman *et al.*, Phys. Rev. B **79**, 024513 (2009).

[22] R. Hoffmann and C. Zheng, J. Phys. Chem. **89**, 4175 (1985).

[23] E. Gustenau, P. Herzig, and A. Neckel, J. Solid State Chem. **129**, 147 (1997).

[24] E. Gustenau, P. Herzig, and A. Neckel, J. Alloys Compd. **262-263**, 516 (1997).

[25] D. Johrendt, C. Felser, O. Jepsen, O. K. Andersen, A. Mewis, and J. Rouxel, J. Solid State Chem. **130**, 254 (1997).

[26] D. J. Singh, Phys. Rev. B **78**, 094511 (2008).

[27] D. J. Singh, Phys. Rev. B **79**, 153102 (2009).

[28] A. Subedi and D. J. Singh, Phys. Rev. B **78**, 132511 (2008).

[29] J. An, A. S. Sefat, D. J. Singh, and M.-H. Du, Phys. Rev. B **79**, 075120 (2009).

[30] C. Huhnt, W. Schlabitz, A. Wurth, A. Mewis, and M. Reehuis, Physica B **252**, 44 (1998).

[31] Y.-Z. Zhang, H. C. Kandpal, I. Ophale, H. O. Jeschke, and R. Valenti, Phys. Rev. B **80**, 094530 (2009).

[32] C. Huhnt, G. Michels, M. Roepke, W. Schlabitz, A. Wurth, D. Johrendt, and A. Mewis, Physica B **240**, 26 (1997).

[33] C. Huhnt, W. Schlabitz, A. Wurth, A. Mewis, and M. Reehuis, Phys. Rev. B **56**, 13796 (1997).

[34] M. Chefki, M. M. Abd-Elmeguid, H. Micklitz, C. Huhnt, W. Schlabitz, M. Reehuis, and W. Jeitschko, Phys. Rev. Lett. **80**, 802 (1998).

[35] B. Ni, M. M. Abd-Elmeguid, H. Micklitz, J. P. Sanchez, P. Vullier, and D. Johrendt, Phys. Rev. B **63**, 100102R (2001).

[36] A. Wurth, D. Johrendt, C. Huhnt, G. Michels, M. Roepke, and W. Schlabitz, Z. Anorg. Allg. Chem. **623**, 1418 (1997).

[37] S. Jia, A. J. Williams, P. W. Stephens, and R. J. Cava, Phys. Rev. B **80**, 165107 (2009).

[38] A. P. Hammersley, S. O. Svensson, M. Hanfland, A. Fitch, and D. Haeusermann, High Press. Res. **14**, 235 (1996).

[39] J. Rodríguez-Carvajal, Physica B **192**, 55 (1993).

[40] K. Koepernik and H. Eschrig, Phys. Rev. B **59**, 1743 (1999).

[41] I. Opahle, K. Koepernik, and H. Eschrig, Phys. Rev. B **60**, 14035 (1999).

[42] M. Kohout, Int. J. Quantum Chem. **97**, 651 (2004).

[43] A. Ormeci, H. Rosner, F. R. Wagner, M. Kohout, and Y. Grin, J. Phys. Chem. A **110**, 1100 (2006).

[44] M. Kohout, BASIN, version 4.7, 2008.

[45] R. F. W. Bader, *Atoms in Molecules: A Quantum Theory* (Oxford University Press, New York, 1990).

[46] Due to technical reasons, we were not able to perform "pressure-down" measurements for $SrFe_2As_2$.

[47] N. Mandel and J. Donohue, Acta Crystallogr. Sec. B **27**, 476 (1971).

[48] D. J. Braun and W. Jeitschko, J. Solid State Chem. **32**, 357 (1980).

[49] J. Donohue, *The Structures of the Elements* (Wiley, New York, 1974).

[50] C. Krellner, N. Caroca-Canales, A. Jesche, H. Rosner, A. Ormeci, and C. Geibel, Phys. Rev. B **78**, 100504(R) (2008).

[51] S. Kimber *et al.*, Nature Mater. **8**, 471 (2009).

[52] T. Yildirim, Phys. Rev. Lett. **102**, 037003 (2009).

[53] See Supplemental Material at http://link.aps.org/supplemental/10.1103/PhysRevB.84.054509 for details regarding the GGA calculations and the effects of z(As) optimization.

[54] Previously (Ref. 31), such a behavior was observed in the calculations when going from the ordered SDW orthorhombic phase to the nonmagnetic tetragonal phase.

[55] I. I. Mazin, M. D. Johannes, L. Boeri, K. Koepernik, and D. J. Singh, Phys. Rev. B **78**, 085105 (2008).

[56] M. D. Johannes and I. I. Mazin, Phys. Rev. B **82**, 024527 (2010).

[57] I. I. Mazin and M. D. Johannes, Nature Phys. **5**, 141 (2009).

[58] L. J. Li *et al.*, New J. Phys. **11**, 025008 (2009).

[59] M. Rotter, C. Hieke, and D. Johrendt, Phys. Rev. B **82**, 014513 (2010).

[60] To avoid any ambiguity from the lack of a “pressure-down” data for $SrFe_2As_2$, we have only taken into account the “pressure-up” data for both $SrFe_2As_2$ and $SrFe_{1.8}Ru_{0.2}As_2$ to compare the transition pressure.

[61] R. Nath, Y. Singh, and D. C. Johnston, Phys. Rev. B **79**, 174513 (2009).

[62] Z. Ban and M. Sikirica, Acta Crystallogr. **18**, 594 (1965).

[63] P. Villars, *Pearson’s Handbook of Crystallographic Data for Intermetallic Phases*, 2nd ed. (ASM International, Materials Park, OH, 1991).

[64] G. Just and P. Paufler, J. Alloys Compd. **232**, 1 (1996).

[65] A. Szytuła and J. Leciejewicz, in *Handbook on the Physics and Chemistry of Rare Earths*, edited by K. A. Gschneidner Jr. and L. Eyring, Vol. 12 (North Holland, Amsterdam, 1989), pp. 133–211.

[66] O. I. Bodak, E. I. Gladyshevskii, and P. I. Kripyakevich, Izv. Akad. Nauk SSSR, Neorg. Mater. **2**, 2151 (1965).

[67] E. Parthé and B. Chabot, *Handbook on the Physics and Chemistry of Rare Earths*, edited by K. A. Gschneidner Jr. and L. Eyring, Vol. 6 (North Holland, Amsterdam, 1984), pp. 113–334.

[68] H. Schlenger, H. Jacobs, and R. Juza, Z. Anorg. Allg. Chem. **385**, 177 (1971).

[69] A. Mewis, Z. Naturforsch. B **32**, 351 (1977).

[70] R. Marchand and W. Jeitschko, J. Solid State Chem. **24**, 351 (1978).

[71] W. Jeitschko and B. Jaberg, J. Solid State Chem. **35**, 312 (1980).

[72] M. Pfisterer and G. Nagorsen, Z. Naturforsch. B **38**, 811 (1983).

[73] W. Jeitschko, R. Glaum, and L. Boonk, J. Solid State Chem. **69**, 93 (1987).

[74] A. Mewis, Z. Naturforsch. B **35**, 141 (1980).

[75] W. Jeitschko and M. Reehuis, J. Phys. Chem. Solids **48**, 667 (1987).

[76] M. Reehuis, W. Jeitschko, G. Kotzyba, B. Zimmer, and X. Hu, J. Alloys Compd. **266**, 54 (1998).

[77] H. Schaefer, B. Eisenmann, and W. Mueller, Angew. Chem. Int. Ed. Engl. **12**, 694 (1973).

[78] W. K. Hofmann and W. Jeitschko, J. Solid State Chem. **51**, 151 (1984).

[79] W. Jeitschko, U. Meisen, M. H. Müller, and M. Reehuis, Z. Anorg. Allg. Chem. **527**, 73 (1985).

[80] W. K. Hofman and W. Jeitschko, Monatsh. Chem. **116**, 569 (1985).

[81] M. Kohout, Faraday Discuss. **135**, 43 (2007).

[82] M. Kohout, F. R. Wagner, and Y. Grin, Int. J. Quantum Chem. **106**, 1499 (2006).

[83] F. R. Wagner, V. Bezugly, M. Kohout, and Y. Grin, Chem. Eur. J. **13**, 5724 (2007).

[84] M. Kohout, F. R. Wagner, and Y. Grin, Theor. Chem. Acc. **108**, 150 (2002).

[85] O. Sichevych, M. Kohout, W. Schnelle, H. Borrman, R. Cardoso-Gil, M. Schmidt, U. Burkhardt, and Y. Grin, Inorg. Chem. **48**, 6261 (2009).

[86] F. R. Wagner, M. Kohout, and Y. Grin, J. Phys. Chem. A **112**, 9814 (2008).

[87] V. Bezugly, P. Wielgus, M. Kohout, and F. R. Wagner, J. Comput. Chem. **31**, 2273 (2010).

[88] W. O. Uhoya, J. M. Montgomery, G. M Tsoi, Y. K. Vohra, M. A McGuire, A. S Sefat, B. C Sales, and S. T. Weir, J. Phys. Condens. Matter **23**, 122201 (2011).